Atmos. Chem. Phys. Discuss., 11, 5351–5378, 2011
www.atmos-chem-phys-discuss.net/11/5351/2011/
doi:10.5194/acpd-11-5351-2011

Atmospheric Chemistry and Physics Discussions

Characterization of wildfire NO_x emissions using MODIS fire radiative power and OMI tropospheric NO_2 columns

A. K. Mebust[1], **A. R. Russell**[1], **R. C. Hudman**[1], **L. C. Valin**[1], **and R. C. Cohen**[1,2]

[1]Dept. of Chemistry, University of California at Berkeley, Berkeley, California, USA
[2]Dept. of Earth and Planetary Science, University of California at Berkeley, Berkeley, California, USA

Received: 14 January 2011 – Accepted: 29 January 2011 – Published: 11 February 2011

Correspondence to: R. C. Cohen (rccohen@berkeley.edu)

Published by Copernicus Publications on behalf of the European Geosciences Union.

Abstract

We use observations of fire radiative power (FRP) from the Moderate Resolution Imaging Spectroradiometer (MODIS) and tropospheric NO_2 column measurements from the Ozone Monitoring Instrument (OMI) to derive NO_2 wildfire emission coefficients ($g\,MJ^{-1}$) for three land types over California and Nevada. Retrieved emission coefficients were 0.279 ± 0.077, 0.342 ± 0.053, and $0.696 \pm 0.088\,g\,MJ^{-1}$ NO_2 for forest, grass and shrub fuels, respectively. These emission coefficients reproduce ratios of emissions with fuel type reported previously using independent methods. However, the magnitude of these coefficients is lower than prior estimates, which suggests either a negative bias in the OMI NO_2 retrieval over regions of active emissions, or that the average fire observed in our study has a smaller ratio of flaming to smoldering combustion than measurements used in prior estimates of emissions. Our results indicate that satellite data can provide an extensive characterization of the variability in fire NO_x emissions; 67% of the variability in emissions in this region can be accounted for using an FRP-based parameterization.

1 Introduction

Emissions from vegetation fires are a significant source of trace gases (e.g. CO, NO_x, VOCs) and particulate matter to the atmosphere (Andreae and Merlet, 2001); formation of secondary pollutants occurs as a result of these emissions with consequences that range from local to global in scale (e.g. Val Martin et al., 2006; Cook et al., 2007; Pfister et al., 2008; Hudman et al., 2009). NO_x ($NO + NO_2$) emissions play a major role both in the production of ozone, a monitored pollutant and tropospheric greenhouse gas, and in the regulation of oxidant concentrations. NO_x emissions from biomass and biofuel burning contribute approximately $5.9\,Tg\,N\,y^{-1}$ to the atmosphere, roughly 15% of the global NO_x budget (Denman et al., 2007), with total emissions from wildfires fluctuating from year to year due to interannual variability in fire frequency and intensity.

ACPD
11, 5351–5378, 2011

However, there are significant uncertainties associated with biomass burning budgets due to the large uncertainties in NO_x emission factors and global biomass burned. For example, Jaegle et al. (2005) partitioned yearly GOME satellite NO_2 data to determine budgets for individual NO_x sources in 2000; while a priori and top-down global inventory totals for fire emissions agreed, regional differences of up to 50% between these two inventories were noted and attributed to uncertainties in regionally resolved NO_x emission factors used in the study. Laboratory studies also indicate that biomass burning NO_x emission factors can vary greatly–even among plants from similar ecosystems or among plants categorized as similar under current emissions inventories, e.g. extratropical forest (McMeeking et al., 2009). These wide variations on regional scales raise questions as to whether existing parameterizations capture the mean emissions from the range of recent fires, and whether a more detailed parameterization could capture some of this variability in emissions.

Biomass burning emissions have generally been estimated using bottom-up estimates (Wiedinmyer et al., 2006):

$$M_X = M_T \times EF_X \quad (1)$$

where M_X is the mass of a species X emitted by the fire, M_T is the total biomass burned, and EF_X is the empirically measured emission factor (EF) for species X, expressed as the ratio of pollutant mass emitted to the total biomass burned. NO_x emissions vary greatly based on individual fire conditions, such as differences in the flaming vs. smoldering fraction of the fuel burned and its nitrogen content; most NO_x EFs used in atmospheric modeling applications are reported with high uncertainties (±50%) as this variability is significant between different biomes and emissions in a given location are attributed to one of only a handful of biome categories (Andreae and Merlet, 2001; Battye and Battye, 2002). NO_x EFs are primarily based on airborne and occasionally local measurements from wildfires or prescribed fires (e.g. Laursen et al., 1992; Goode et al., 2000; Yokelson et al., 2007; Alvarado et al., 2010), or measurements from small fires burned under controlled laboratory conditions (e.g. Goode et al., 1999; Freeborn et al., 2008; Yokelson et al., 2008; McMeeking et al., 2009). Airborne measurements,

ACPD
11, 5351–5378, 2011

while precise for a given fire, face obvious limitations with respect to the number and size of fires that can be sampled, limiting their ability to characterize variability in fire emissions on regional scales; these measurements may also oversample the contribution of flaming emissions to total fire emissions (van Leeuwen and van der Werf, 2010). Laboratory fires, on the other hand, do not accurately recreate several characteristics of typical large-scale natural wildfires including size, fuel moisture, flaming and smoldering fractions, and structural and meteorological characteristics, among others. Satellite measurements offer an opportunity to bridge the gap between global analyses that identify a need for representative emission factors at regional scales and observations at the fuel and individual fire level.

In the mass-burned formalism M_T is estimated as

$$M_T = A \times B \times C \quad (2)$$

where A is the burned area, B is the available fuel per unit area, and C is the combustion completeness, or fraction of available fuel that was burned (Seiler and Crutzen, 1980; Wiedinmyer et al., 2006). Poor knowledge of A, B and C leads to large uncertainties in the mass of pollutant emitted, and the lack of temporal and spatial resolution prevents air quality forecasting of individual fires in real time (Ichoku and Kaufman, 2005). In recent literature, a linear relationship between the biomass burned in a fire and the radiative energy released by the fire has been established (Wooster, 2002; Wooster et al., 2005; Freeborn et al., 2008), leading to a new expression of pollutant mass emission:

$$M_X = \mathrm{EC}_X \times E_R = K \times \mathrm{EF}_X \times E_R \quad (3)$$

where EC_X is an "emission coefficient" (EC) expressed as the mass of pollutant emitted per unit of radiative energy, E_R is the total radiative energy, and K is an empirically measured coefficient with reported uncertainties of approximately 10–15% (Ichoku and Kaufman, 2005; Wooster et al., 2005; Vermote et al., 2009). E_R can be measured remotely and so may have lower uncertainties than estimates of mass burned for larger

ACPD
11, 5351–5378, 2011

fires; thus some recent studies of fire emissions have focused on directly establishing EC_X for pollutants of interest (Ichoku and Kaufman, 2005; Freeborn et al., 2008; Jordan et al., 2008; Vermote et al., 2009). Although NO_x ECs have been measured for small experimental fires (Freeborn et al., 2008), they may not accurately represent emissions for larger scale natural fires, and only a small number of fuel types are represented. Satellite observations with relatively high spatiotemporal resolution provide us the opportunity to directly measure NO_x ECs and to gather statistics of variation among wildfires using observations from a large number of fires.

Here we show that satellite observations of fire activity and NO_2 can establish statistical properties of NO_2 ECs. We evaluate emissions from 1960 fires in California and Nevada over the years 2005–2008 to derive NO_2 ECs for three land cover classes (forest, shrub and grass) by combining NO_2 columns from the Ozone Monitoring Instrument (OMI) aboard NASA's EOS-Aura satellite, wind vectors from the North American Regional Reanalysis (NARR), and measurements of fire radiative power (FRP) from the Moderate Resolution Imaging Spectroradiometer (MODIS) instrument on NASA's EOS-Aqua satellite. Although not considered a major contributor to global biomass burning emissions, this region has a number of fires over diverse land types which can aid our understanding of variations in emissions with fuel type. Further, emissions from individual fires in this region can significantly perturb NO_x levels over the natural background, leading to local and regional degradation of air quality (Pfister et al., 2008). We note that in this paper, the phrases "NO_2 emissions" and "NO_2 ECs" refer to emissions and ECs derived from the observed NO_2 columns, and thus represent total NO_2 present in plumes at NO-NO_2 photostationary state, as opposed to direct NO_2 emissions from fires.

2 Datasets

The MODIS instruments reside on the NASA EOS-Terra and EOS-Aqua satellites, measuring spectral radiance from Earth; the MODIS fire detection algorithm employs

ACPD
11, 5351–5378, 2011

infrared spectral channels at 4 and 11 µm (Kaufman et al., 1998). We use daytime fire detections at 1 km nominal resolution from the MODIS Aqua Thermal Anomalies Level 2 Collection 5 data product, MYD14 (Giglio et al., 2003). FRP is provided for each fire pixel via an empirical relationship using the 4 µm band brightness temperatures (Kaufman et al., 1998; Justice et al., 2002). Sensitivity studies indicate that the theoretical average standard error associated with this relationship is ±16%, and is higher for small fires and lower for more energetic fires (Kaufman et al., 1998). Independent validation by Wooster et al. (2003) using the Bi-spectral InfraRed Detection satellite instrument found that the two instruments agreed to within 15% for some fires but that MODIS underestimates FRP by up to 46% for fires that include less intensely radiating fire pixels which are not detected by the MODIS algorithm. To identify the primary land type for each fire pixel we use the MODIS Aqua+Terra Land Cover Level 3 Collection 5 (MCD12Q1) product, which provides yearly land cover classification at 500 m × 500 m resolution (Friedl et al., 2010).

To measure NO_2 emissions we use tropospheric vertical column densities of NO_2 obtained from the OMI NO_2 standard product (Level 2, Version 1.0.5, Collection 3) available from the NASA Goddard Earth Sciences (GES) Data and Information Services Center (DISC). OMI is a nadir-viewing spectrometer, measuring backscattered solar radiation from earth at UV and visible wavelengths (270–500 nm) with a spectral resolution of ∼ 0.5 nm. OMI employs differential optical absorption spectroscopy (DOAS) to measure NO_2; the tropospheric vertical columns of NO_2 and corresponding standard errors used in this work are retrieved as described by Boersma et al. (2004), Bucsela et al. (2006), and Celarier et al. (2008). With daily global coverage at a spatial resolution of 13 km × 24 km at nadir, OMI has the highest resolution of any remote instrument measuring NO_2 columns. In this work, only the 40 inner pixels out of 60 total (in the across-track direction) were used, minimizing effects of poor resolution in the outer, larger pixels. OMI pixels with cloud fractions greater than 20% were not included in our analysis to reduce uncertainties associated with cloud cover (Boersma et al., 2002; Celarier et al., 2008).

ACPD
11, 5351–5378, 2011

We use wind fields at 900 hPa (~ 1 km) from NARR, a data assimilation system that provides meteorological variables at 32 km horizontal resolution and 45 vertical layers every three hours from 1979–present (Mesinger et al., 2006). MODIS, OMI and NARR data for each fire were collocated in time to within one hour.

3 Methods

We follow the method outlined by Ichoku and Kaufman (2005), which computes regional ECs globally for smoke aerosol in 2002, with several significant modifications to calculate ECs for NO_2 as described below. We begin with a brief summary of the method presented in the aforementioned study so as to highlight our modifications.

In the original study, Ichoku and Kaufman (2005) first collocated MODIS aerosol pixels and MODIS fire detections. For each MODIS aerosol pixel identified as containing fire, a series of calculations were performed; first, the aerosol optical thickness (AOT) contributed by fire emissions was measured by subtracting the minimum AOT of the aerosol pixel containing fire and the eight surrounding aerosol pixels from the maximum AOT of these same pixels. Next, the authors converted AOT to column mass density, a step not required in our analysis as the OMI standard product provides NO_2 column mass densities directly. Ichoku and Kaufman (2005) then calculated the wind speed over the pixel and a characteristic length over which the wind must blow to clear the region of aerosol; this was given as the square root of the area of the aerosol pixel, which was assumed to be square. Using this characteristic length and the wind speed, a clear time (see below) is given; the smoke mass emission rate is then given by the total mass of aerosol contributed by fire emissions divided by this clear time. Ichoku and Kaufman (2005) then grouped aerosol pixels by their proximity and averaged these values for all pixels in a group.

We now present our method in detail, with significant deviations from Ichoku and Kaufman (2005) which are highlighted at the end of this section. Fire detections over California and Nevada and surrounding areas (31–44° N, 126–113° W) from 2005–

ACPD
11, 5351–5378, 2011

2008 were assigned a primary fuel type of forest, shrub, grass or "other" (including sparsely vegetated, urban, or agricultural land) using the MODIS land cover product from the corresponding year (see Fig. 1a). For each day, OMI pixels and fire pixels were grouped into fire "events" such that adjacent OMI pixels containing fires were grouped together and rectangular regions were defined around each event (see Fig. 1b). Each event then represents all fire pixels in that location from a single day of observation, where the fire pixels are close enough to each other that the OMI spatial resolution cannot separately resolve their emissions.

The total mass emitted by each fire as measured by OMI was calculated as follows: total OMI tropospheric NO_2 columns for each event ($X_{NO_2,f}$) were obtained by averaging all columns in the rectangular region, weighted by pixel area, with the column standard deviation ($\sigma_{NO_2,f}$) equal to the weighted average of column standard deviations reported in the retrieval. OMI columns over the rectangular region were measured in a similar way for 60 days before and after the fire; the average of these columns yielded an event background NO_2 column ($X_{NO_2,b}$) with corresponding background column standard deviation ($\sigma_{NO_2,b}$). Columns containing MODIS fire detections were eliminated from the background average. The total mass of NO_2 emitted by the fire M_{NO_2} (in kg) was then given by

$$M_{NO_2} = (X_{NO_2,f} - X_{NO_2,b}) \times A_R \quad (4)$$

where A_R is the regional area. The standard deviation for M_{NO_2} is given by

$$\sigma_{NO_2} = (\sigma_{NO_2,f} - \sigma_{NO_2,b}) \times A_R \quad (5)$$

As FRP is the rate of radiative energy release ($MJ\,s^{-1}$), the next step in the analysis was to determine the time over which the measured mass of NO_2 had been emitted. The time for emitted NO_2 to clear the region (t_c) was derived using wind speed (w) and direction from NARR wind fields at 900 mb (~ 1 km):

$$t_c = d_c w^{-1}, \quad (6)$$

ACPD
11, 5351–5378, 2011

where d_c is the distance from the center of the fire to the edge of the region along the wind direction. Standard error in d_c was assumed to be at least 2 km (twice the nominal resolution of a MODIS pixel) and for larger fires, was given as the standard error associated with measuring the center of the fire; the center was found as an average of all fire pixel locations for that fire, weighted by FRP. Uncertainties in wind speed and direction for individual data points were difficult to assess and quantify, and as a result were neglected; percent standard error in t_c was assumed equal to percent standard error in d_c. For each event, dividing M_{NO_2} by t_c yielded a mass emission rate (MER) of NO_2 for the region, with percent standard error equal to percent standard error from t_c and M_{NO_2}, summed in quadrature. Summing pixel FRP for each land type yielded the total event FRP for each land type (in MJ), with standard error estimated at 30%, between 15% and 46% as reported in Wooster et al. (2003).

Satellite observations of fire emissions will necessarily contain a mixture of fresh and aged smoke, due to the spatial resolution of the observing instrument. NO_x is a relatively short-lived species; observations and theoretical studies both support the notion that NO_x concentrations in a fire plume will decay with time due to the formation of nitric acid (HNO_3) and NO_x reservoir species such as peroxyacetyl nitrate (PAN) (e.g. Jacob et al., 1992; Mauzerall et al., 1998; Leung et al., 2007; Real et al., 2007; Alvarado et al., 2010). Thus, the aged smoke present in satellite observations will bias our measured ECs low. To evaluate this effect, we consider a 1-D model of a fire plume, assuming a constant wind speed along the dependent axis; horizontal diffusion and vertical distribution of emissions are neglected. We also assume first-order reaction kinetics for NO_x, governed by a rate constant k; the lifetime is $\tau = k^{-1}$. The concentration of NO_2 as a function of distance from the fire is then:

$$C(x) = C_0 \exp(-kw^{-1}x), \quad (7)$$

where C_0 is the concentration immediately over the source (kg m−1 in our 1-D model) and x is the distance downwind from the source. Note that since we assume a constant wind speed, the age of the smoke at x is given by $t = w^{-1}x$. The satellite will observe all NO_2 between the source and some point x_0 which represents the edge of the satellite

ACPD
11, 5351–5378, 2011

pixel, and the total mass observed is equal to the integral of NO_2 concentration from the origin to x_0:

$$M_{NO_2} = \int_0^{x_0} C(x)dx = C_0 \int_0^{x_0} \exp(-kw^{-1}x)\, dx = C_0 w k^{-1} [1 - \exp(-kw^{-1}x_0)]. \quad (8)$$

Here, the clear time, t_c, is defined as the time required for transport from the source to the edge of the pixel: $t_c = w^{-1}x_0$. We also note that C_0x_0 corresponds to the total mass that would be observed had no decay in NO_2 occurred; thus $C_0x_0t_c^{-1}$ is equal to the mass emission rate that would have been measured with no decay, or equivalently, the initial mass emission rate at the fire source, MER_{init}. We can thus rewrite our total mass observed equation as:

$$M_{NO_2} = C_0x_0t_c^{-1}k^{-1}[1 - \exp(-kt_c)] = MER_{init}\tau[1 - \exp(-\tau^{-1}t_c)]. \quad (9)$$

Dividing both sides by t_c yields our measured MER as a function of the initial MER, lifetime τ, and clear time t_c:

$$MER_{meas} = MER_{init}\tau t_c^{-1}[1 - \exp(-\tau^{-1}t_c)]. \quad (10)$$

Although this 1-D model neglects diffusion, in most cases the width of the rectangular region is large enough that horizontal diffusion does not remove the fire-emitted NO_2 from the satellite field of view; thus this is a useful first order approximation of the relationship between initial and measured MER. We use this equation to apply a chemistry correction factor to each point in our analysis, assuming an appropriate lifetime.

Previous studies offer a range of NO_x lifetimes within fire plumes. Observations of NO_x and reaction products measured during ARCTAS and reported in Alvarado et al. (2010) indicate a NO_x lifetime of 2–3 h, as does the photochemical model presented in Yokelson et al. (1999). Spichtinger et al. (2001) varied NO_x lifetimes in FLEXPART simulations of a fire NO_x plume and found that using a lifetime of 9 h (the minimum lifetime tested) still overpredicted NO_2 columns observed by GOME by a factor of 2.

ACPD
11, 5351–5378, 2011

Jacob et al. (1992) used a Lagrangian plume model to reconstruct photochemistry in observed aged biomass burning plumes, and found a NO_x lifetime of 5–7 h. However, these two studies are based on model output and not direct observational data. We select a lifetime of 2 h, which is in agreement with observations. A plot of MER decay for three different clear times (the time required to exit the satellite pixel) is shown in Fig. 2. These three clear times (5 min, 55 min, and 3 h) represent a short, average, and long clear time for our analysis, respectively. At a lifetime of 2 h, the apparent MER that would be inferred from the satellite observations for the average case is biased low by 20%. Longer lifetimes result in less bias. Thus our choice of lifetime introduces at most a minor bias unless the lifetime is shorter than 45 min. We apply the correction to each point as a function of clear time, and assume an uncertainty from this correction equal to the percent difference between the measured and corrected MERs; overall uncertainty in the corrected MER is then obtained by summing in quadrature this uncertainty with the measured MER uncertainty.

A series of filters was required to ensure high data quality. All events with a background column greater than 3.5×10^{15} molecules cm^{-2} were omitted from further analysis as it was difficult to distinguish fire emissions from variations in the background anthropogenic emissions of NO_x (361 points). Events with a clear time of greater than 3 h were removed to reduce errors associated with changes in FRP or wind speed and direction during the transit time (199 points from the remaining dataset). Events from a region near Santa Barbara (34–35° N, 118–121° W) were also removed, due to errors in wind noticed over this region and likely associated with unresolved Santa Ana winds (37 points). Finally, points that had both high percent uncertainty (> 100%) and high absolute uncertainty ($> 1\,kg\,s^{-1}$) in MER were removed (430 points); this preserved points with MER near zero and a high percent uncertainty but low overall uncertainty. Overall, 34% of data points were removed via filtering; 1960 events remained for this analysis.

We identified several aspects of the study by Ichoku and Kaufman (2005) that did not translate to the OMI NO_2 observations. The method used by

ACPD
11, 5351–5378, 2011

Ichoku and Kaufman (2005) to measure total and background mass overestimated emitted NO_2 when applied to our dataset, due to regional variation in NO_x concentrations on the spatial scale of an OMI pixel; hence our development of the new method described above to account for these variations. This method analyzes several pixels at once, so there was also no need to include an averaging step at the end of the analysis. We also use a more precise determination of the characteristic length using the direction of the wind and the center of the fire, as well as a higher resolution wind dataset (NARR at 32 km resolution instead of the NCEP global reanalysis at $2^{\circ} \times 2.5^{\circ}$). The study presented by Ichoku and Kaufman (2005) performed regional and subregional analyses over the globe, and assumed these subregions were representative of a single fuel type; we instead applied the MODIS Land Cover product to individual fire pixels. Our correction to account for photochemical processing of the measured smoke plume is also a necessary correction for NO_x which in smoke plumes has a very short lifetime; this correction was not included in the original study by Ichoku and Kaufman (2005).

4 Results and discussion

Figure 3 shows FRP vs. MER for all fires, as well as fires separated by their primary fuel type. Fires were identified as forest, grass, or shrub fires if at least 75% of FRP came from fire pixels of that fuel type. Best fit lines (with intercept fixed at zero) and R^2 values are shown. Distinctly different slopes are measured for all three fuel types, and with the exception of forest fires, analyzing emissions separated by fuel type improves the correlation coefficient. Forest fires exhibit more variability in emissions than other fuel types; this may be due to contributions from grass or shrub burning in forest-type pixels, or greater variation in extent of flaming combustion during which most NO_x is emitted. The small number of larger fires (only four fires with FRP > 5000 MJ) may also have an effect, as percent uncertainty in FRP is likely greater for small fires (Kaufman et al., 1998).

ACPD
11, 5351–5378, 2011

Limiting the analysis to individual fuel types reduces its statistical rigor. To obtain ECs with well-characterized uncertainties and including all of the data deemed reliable, a multiple regression with nonparametric bootstrap resampling was used. Since the emission parameterization scales linearly, the MER equation can be expanded to vary linearly with landtype:

$$\mathrm{MER} = (\mathrm{FRP_F} \times \mathrm{EC_F}) + (\mathrm{FRP_G} \times \mathrm{EC_G}) + (\mathrm{FRP_S} \times \mathrm{EC_S}) \quad (11)$$

where F, G and S correspond to forest, grass and shrub land types. Points were randomly sampled with replacement and the multiple regression on land type FRP was performed 300000 times; the resulting averaged ECs (in $\mathrm{g\,MJ^{-1}\,NO_2}$) and their standard deviations (Table 1) were used to calculate predicted MERs for each fire measured in the analysis, as shown in Fig. 4. The best fit line (slope of 0.988) demonstrates that these ECs appropriately reproduce overall emissions. The correlation coefficient indicates that this parameterization method accounts for approximately 67% of the variability in emissions on this scale.

Previously, $\mathrm{NO_x}$ EFs of 2.5 ± 1.2 for forests, 3.5 ± 0.9 for grass and 6.5 ± 2.7 ($\mathrm{g\,kg^{-1}}$) for shrubs were reported for fires in North America by Battye and Battye (2002). As a ratio to the forest fire emissions, these reported $\mathrm{NO_x}$ EFs are 2.4 times higher for shrub fires and 1.6 for grass fires, mainly reflecting differences in the C:N ratios of the fuels and differences in typical combustion efficiency. Our analysis gives ECs that are 2.5 times larger for shrub fires and 1.2 times larger for grass fires than forest fires, consistent with those reported by Battye and Battye (2002). Globally averaged $\mathrm{NO_x}$ EFs presented in Andreae and Merlet (2001) do not include a shrub category, but the ratio of the grassland EF to the extratropical forest EF is 1.3 to 1; the grassland number was later revised down by 40% (Hoelzemann et al., 2004), however, a number of papers have provided evidence that the extratropical forest EF should also be revised downward (Spichtinger et al., 2001; Cook et al., 2007; Alvarado et al., 2010).

To directly compare to previously reported $\mathrm{NO_x}$ ECs and EFs, we can convert using a photostationary state $\mathrm{NO/NO_2}$ ratio and the aforementioned proportionality constant

ACPD
11, 5351–5378, 2011

K, the ratio of biomass burned to FRE. For this comparison we assume the plume NO_x is 75% NO_2, as the vast majority of fire plumes observed at OMI resolution are aged long enough for NO and NO_2 to reach photostationary state. This value is also consistent with previous observed and modeled values in fire plumes (Laursen et al., 1992; Alvarado and Prinn, 2009). We estimate that this value is accurate to within 20%. We also use $K = 0.41\,\mathrm{kg\,MJ^{-1}}$, the average of two values measured in previous studies (Wooster et al., 2005; Freeborn et al., 2008). This value was used in Vermote et al. (2009) and the uncertainty estimated to be at least 10%. The resulting NO_x EFs and ECs are presented in Table 1, in kg NO_x (as NO); we note that the overall bias induced by these conversions may be as high as 25% in either direction.

Most reported NO_x emission factors are substantially larger than the ones we derive here. The NO_x EFs reported by Battye and Battye (2002) are roughly 3 times larger than our derived EFs. The grassland EF ($2.32\,\mathrm{g\,kg^{-1}}$) revised from Andreae and Merlet (2001) and given in Hoelzemann et al. (2004) is also roughly 3 times larger than our reported grassland EF and the extratropical forest EF ($3.0\,\mathrm{g\,kg^{-1}}$) from Andreae and Merlet (2001) is 5 times larger than our reported forest EF. Alvarado et al. (2010) used observations of NO_x in boreal forest fire plumes to obtain an emission factor for NO_x of $1.06\,\mathrm{g\,kg^{-1}}$, almost twice our extratropical forest EF, with a reported uncertainty of $\sim 100\%$. Freeborn et al. (2008) report an overall NO_x EC of $1.19 \pm 0.65\,\mathrm{g\,MJ^{-1}}$ for laboratory fires of a number of different fuel types, 2-5 times greater than the NO_x ECs measured in this work ($0.243–0.605\,\mathrm{g\,MJ^{-1}}$).

A number of factors may be responsible for a bias in our measured values; these factors are presented in Table 2, and we discuss them here at length. First, we note that any assumptions we made about average fire behavior, such as NO_x lifetime within the plume, NO_2/NO_x ratio, or the value for K, are a possible source of systematic error, with under- and overestimation being equally likely; however, each of these sources is expected to induce less than 20% error unless a typical NO_x lifetime in a fire plume is less than 1 h. A second source of systematic error is the diurnal cycle of fire behavior. A number of studies indicate that fire activity peaks in the afternoon (Giglio, 2007;

ACPD
11, 5351–5378, 2011

Zhang and Kondragunta, 2008; Vermote et al., 2009). Data presented in Vermote et al. (2009) and Zhang and Kondragunta (2008) suggests that average activity increases roughly linearly from morning to peak activity. Our analysis assumes constant FRP throughout the time over which emissions were measured for each data point; while some fires will increase in FRP over this time and some fires will decrease, the diurnal cycles presented in these studies suggest that on average we are overestimating FRP by up to 20%, depending on the average clear time.

To verify this effect, we analyzed all points in our analysis that were also detected during the morning overpass of MODIS on the Terra satellite, approximately 25% of the fires we studied, including the majority of large fires. For each point, we assumed FRP varied linearly from the Terra overpass to the Aqua overpass, and using the clear time, calculated the average FRP over the time of our measurement. Bootstrapping with these average FRPs instead of the Aqua FRP resulted in shrub and grass EFs approximately 15% greater than those presented in this work, indicating a small low bias. The forest EF increased by 40%, a much larger effect, but it is not clear that this is statistically significant.

There are also some sources of systematic error that would bias our measured numbers high including underestimation of FRP by MODIS due to clouds, smoke or canopy cover (Vermote et al., 2009); as discussed previously, this bias can be as high as 50% for some individual fires, but an average bias is likely 15–30% (Wooster et al., 2003). Also, it is possible that since our observations occur close to the peak in fire activity, the fires we observe may be more heavily weighted towards flaming emissions than an average wildfire, and thus are biased high. Since most wildfires are a mix of flaming and smoldering components, we estimate that bias from this source is 10–20%. Winds also represent a possible source of error due to variations in plume height and accuracy and spatiotemporal resolution of the reanalysis; however, these errors are expected to be random and small relative to other errors and thus should not contribute a bias. A summary of all quantified potential biases is presented in Table 2, in the first six rows. Summing these biases suggests that our values are actually likely to be biased high by

ACPD
11, 5351–5378, 2011

approximately 5–35%, with potential bias ranging from 50% underestimation to 90% overestimation. This bias is small compared to the difference between our emission coefficients and prior estimates, and probably in the opposite direction.

One possible explanation for the difference is that previous in situ and laboratory studies overestimate NO_x emissions from wildfires, due to oversampling of flaming emissions in the laboratory or from airborne platforms; another possibility is that emissions from wildfires in California are lower than emissions used to derive prior estimates.

Alternatively, we might interpret these results to indicate that there is a bias in the OMI retrieval process over wildfires. The NO_2 tropospheric column retrieval does not account for differences in NO_2 vertical profile and aerosol loading associated with wildfire conditions, nor does it explicitly account for effects of aerosol loading due to fires, both of which can act to systematically bias NO_2 columns over wildfires. Most analyses suggest the bias due to aerosol is relatively minor ($< 20\%$), as aerosol is treated implicitly as part of the cloud correction (Boersma et al., 2004). Uncertainty due to profile shape is more difficult to constrain, as NO_2 profile data is sparse; Lamsal et al. (2010) indicate that biases between the OMI standard product and ground based measurements range from −5.6% to 71%, and they attribute much of this difference to profile error. Simultaneous in situ and satellite observation of NO_2 in plumes would be extremely useful as a constraint. Despite our inability to quantify these biases, we include uncharacteristically low CA emissions and a bias in the OMI retrieval in Table 2.

5 Conclusions

We derive NO_2 ECs (in $g\,MJ^{-1}\,NO_2$) for wildfires in California and Nevada using satellite measurements of NO_2 column densities and fire radiative energy. ECs for forest, shrub and grass fuels were found to be 0.279 ± 0.077, 0.696 ± 0.088, and $0.342 \pm 0.053\,g\,MJ^{-1}\,NO_2$, respectively, with reported uncertainties equal to the standard deviation in the measurement. The variation of these ECs with land type

ACPD
11, 5351–5378, 2011

reproduces ratios seen in previous work; however, these ECs are significantly lower than previously reported emissions estimates. Systematic biases in assumptions within the analysis and in FRP measurement may bias these values low by up to 33%, an amount too small to explain these differences. We conclude either: (a) there exists a large (50–100%) negative bias in the OMI retrieval of NO_2 columns over wildfire plumes, presumably due to errors in assumed profile shape; (b) NO_x emissions from fires in California are lower on average than those represented by previously reported EFs; or (c) these previously reported EFs are overestimated, due to oversampling of flaming combustion by in situ measurements. Whatever the source of these differences, the parameters derived here are unambiguously a lower bound on fire NO_x emissions.

Acknowledgements. This work was supported by the National Aeronautics and Space Administration, grant NNX08AE566, and by an award from the Department of Energy (DOE) Office of Science Graduate Fellowship Program (DOE SCGF). The DOE SCGF Program was made possible in part by the American Recovery and Reinvestment Act of 2009. The DOE SCGF program is administered by the Oak Ridge Institute for Science and Education (ORISE) for the DOE. ORISE is managed by Oak Ridge Associated Universities (ORAU) under DOE contract number DE-AC05-06OR23100. All opinions expressed in this paper are the authors' and do not necessarily reflect the policies and views of DOE, ORAU, or ORISE. OMI data used in this effort were acquired as part of the activities of NASA's Science Mission Directorate, and are archived and distributed by the Goddard Earth Sciences (GES) Data and Information Services Center (DISC). MODIS data are distributed by the Land Processes Distributed Active Archive Center (LP DAAC), located at the U.S. Geological Survey (USGS) Earth Resources Observation and Science (EROS) Center (http://lpdaac.usgs.gov). NARR data were obtained through the NOAA National Operational Model Archive & Distribution System (NOMADS).

ACPD
11, 5351–5378, 2011

References

Alvarado, M. J. and Prinn, R. G.: Formation of ozone and growth of aerosols in young smoke plumes from biomass burning: 1. Lagrangian parcel studies, J. Geophys. Res., 114, D09306, doi:10.1029/2008JD011144, 2009.

Alvarado, M. J., Logan, J. A., Mao, J., Apel, E., Riemer, D., Blake, D., Cohen, R. C., Min, K.-E., Perring, A. E., Browne, E. C., Wooldridge, P. J., Diskin, G. S., Sachse, G. W., Fuelberg, H., Sessions, W. R., Harrigan, D. L., Huey, G., Liao, J., Case-Hanks, A., Jimenez, J. L., Cubison, M. J., Vay, S. A., Weinheimer, A. J., Knapp, D. J., Montzka, D. D., Flocke, F. M., Pollack, I. B., Wennberg, P. O., Kurten, A., Crounse, J., Clair, J. M. St., Wisthaler, A., Mikoviny, T., Yantosca, R. M., Carouge, C. C., and Le Sager, P.: Nitrogen oxides and PAN in plumes from boreal fires during ARCTAS-B and their impact on ozone: an integrated analysis of aircraft and satellite observations, Atmos. Chem. Phys., 10, 9739–9760, doi:10.5194/acp-10-9739-2010, 2010.

Andreae, M. O. and Merlet, P.: Emission of trace gases and aerosols from biomass burning, Global Biogeochem. Cyc., 15, 955–966, 2001.

Battye, W. and Battye, R.: Development of emissions inventory methods for wildland fire, US Environmental Protection Agency, Research Triangle Park, N.C., Contract 68-D-98-046, 2002.

Boersma, F., Bucsela, E., Brinksma, E., and Gleason, J. F.: NO_2, in: OMI Algorithm Theoretical Basis Document, Vol. IV: OMI Trace Gas Algorithms, 2, edited by: Chance, K., Smithsonian Astrophysical Observatory, Cambridge, MA, 13–36, 2002.

Boersma, K. F., Eskes, H. J., and Brinksma, E. J.: Error analysis for tropospheric NO_2 retrieval from space, J. Geophys. Res.-Atmos., 109, D04311, doi:10.1029/2003JD003962, 2004.

Bucsela, E. J., Celarier, E. A., Wenig, M. O., Gleason, J. F., Veefkind, J. P., Boersma, K. F., and Brinksma, E. J.: Algorithm for NO_2 vertical column retrieval from the ozone monitoring instrument, IEEE Trans. Geosci. Remote Sens., 44, 1245–1258, 2006.

Celarier, E. A., Brinksma, E. J., Gleason, J. F., Veefkind, J. P., Cede, A., Herman, J. R., Ionov, D., Goutail, F., Pommereau, J. P., Lambert, J. C., van Roozendael, M., Pinardi, G., Wittrock, F., Schonhardt, A., Richter, A., Ibrahim, O. W., Wagner, T., Bojkov, B., Mount, G., Spinei, E., Chen, C. M., Pongetti, T. J., Sander, S. P., Bucsela, E. J., Wenig, M. O., Swart, D. P. J., Volten, H., Kroon, M., and Levelt, P. F.: Validation of ozone monitoring instrument nitrogen dioxide columns, J. Geophys. Res., 113, D15S15, doi:10.1029/2007JD008908, 2008.

ACPD
11, 5351–5378, 2011

Cook, P. A., Savage, N. H., Turquety, S., Carver, G. D., O'Connor, F. M., Heckel, A., Stewart, D., Whalley, L. K., Parker, A. E., Schlager, H., Singh, H. B., Avery, M. A., Sachse, G. W., Brune, W., Richter, A., Burrows, J. P., Purvis, R., Lewis, A. C., Reeves, C. E., Monks, P. S., Levine, J. G., and Pyle, J. A.: Forest fire plumes over the North Atlantic: p-TOMCAT model simulations with aircraft and satellite measurements from the ITOP/ICARTT campaign, J. Geophys. Res., 112, D10S43, doi:10.1029/2006JD007563, 2007.

Denman, K. L., Brasseur, A., Chidthaisong, A., Ciais, P., Cox, P. M., Dickinson, R. E., Hauglustaine, D., Heinze, C., Holland, E., Jacob, D., Lohmann, U., Ramachandran, S., da Silva Dias, P. L., Wofsy, S. C., and Zhang, X.: Couplings Between Changes in the Climate System and Biogeochemistry, in: Climate Change 2007: The Physical Science Basis, Contribution of Working Group I to the Fourth Assessment Report of the Intergovernmental Panel on Climate Change, edited by: Solomon, S., Qin, D., Manning, M., Chen, Z., Marquis, M., Averyt, K. B., Tignor, M., and Miller, H. L., Cambridge University Press, Cambridge, United Kingdom and New York, NY, USA, 499–588, 2007.

Freeborn, P. H., Wooster, M. J., Hao, W. M., Ryan, C. A., Nordgren, B. L., Baker, S. P., and Ichoku, C.: Relationships between energy release, fuel mass loss, and trace gas and aerosol emissions during laboratory biomass fires, J. Geophys. Res., 113, D01301, doi:10.1029/2007JD008679 , 2008.

Friedl, M. A., Sulla-Menashe, D., Tan, B., Schneider, A., Ramankutty, N., Sibley, A., and Huang, X. M.: MODIS Collection 5 global land cover: Algorithm refinements and characterization of new datasets, Remote Sens. Environ., 114, 168–182, 2010.

Giglio, L.: Characterization of the tropical diurnal fire cycle using VIRS and MODIS observations, Remote Sens. Environ., 108, 407–421, 2007.

Giglio, L., Descloitres, J., Justice, C. O., and Kaufman, Y. J.: An enhanced contextual fire detection algorithm for MODIS, Remote Sens. Environ., 87, 273–282, 2003.

Goode, J. G., Yokelson, R. J., Susott, R. A., and Ward, D. E.: Trace gas emissions from laboratory biomass fires measured by open-path Fourier transform infrared spectroscopy: Fires in grass and surface fuels, J. Geophys. Res.-Atmos., 104, 21237–21245, 1999.

Goode, J. G., Yokelson, R. J., Ward, D. E., Susott, R. A., Babbitt, R. E., Davies, M. A., and Hao, W. M.: Measurements of excess O_3, CO_2, CO, CH_4, C_2H_4, C_2H_2, HCN, NO, NH_3, HCOOH, CH_3COOH, HCHO, and CH_3OH in 1997 Alaskan biomass burning plumes by airborne fourier transform infrared spectroscopy (AFTIR), J. Geophys. Res., 105, 22147–22166, 2000.

Hoelzemann, J. J., Schultz, M. G., Brasseur, G. P., Granier, C., and Simon, M.: Global Wild-

ACPD
11, 5351–5378, 2011

land Fire Emission Model (GWEM): Evaluating the use of global area burnt satellite data, J. Geophys. Res.-Atmos, 109, D14S04, doi:10.1029/2003JD003666, 2004.
Hudman, R. C., Murray, L. T., Jacob, D. J., Turquety, S., Wu, S., Millet, D. B., Avery, M., Goldstein, A. H., and Holloway, J.: North American influence on tropospheric ozone and the effects of recent emission reductions: Constraints from ICARTT observations, J. Geophys. Res., 114, D07302, doi:10.1029/2008JD010126, 2009.
Ichoku, C. and Kaufman, Y. J.: A method to derive smoke emission rates from MODIS fire radiative energy measurements, IEEE Trans. Geosci. Remote Sens., 43, 2636–2649, 2005.
Jacob, D. J., Wofsy, S. C., Bakwin, P. S., Fan, S. M., Harriss, R. C., Talbot, R. W., Bradshaw, J. D., Sandholm, S. T., Singh, H. B., Browell, E. V., Gregory, G. L., Sachse, G. W., Shipham, M. C., Blake, D. R., and Fitzjarrald, D. R.: Summertime Photochemistry of the Troposphere at High Northern Latitudes, J. Geophys. Res., 97, 16421–16431, 1992.
Jaegle, L., Steinberger, L., Martin, R. V., and Chance, K.: Global partitioning of NO_x sources using satellite observations: Relative roles of fossil fuel combustion, biomass burning and soil emissions, Faraday Disc., 130, 407–423, 2005.
Jordan, N. S., Ichoku, C., and Hoff, R. M.: Estimating smoke emissions over the US Southern Great Plains using MODIS fire radiative power and aerosol observations, Atmos. Environ., 42, 2007–2022, 2008.
Justice, C. O., Giglio, L., Korontzi, S., Owens, J., Morisette, J. T., Roy, D., Descloitres, J., Alleaume, S., Petitcolin, F., and Kaufman, Y.: The MODIS fire products, Remote Sens. Environ., 83, 244–262, 2002.
Kaufman, Y. J., Justice, C. O., Flynn, L. P., Kendall, J. D., Prins, E. M., Giglio, L., Ward, D. E., Menzel, W. P., and Setzer, A. W.: Potential global fire monitoring from EOS-MODIS, J. Geophys. Res., 103, 32215–32238, 1998.
Lamsal, L. N., Martin, R. V., van Donkelaar, A., Celarier, E. A., Bucsela, E. J., Boersma, K. F., Dirksen, R., Luo, C., and Wang, Y.: Indirect validation of tropospheric nitrogen dioxide retrieved from the OMI satellite instrument: Insight into the seasonal variation of nitrogen oxides at northern midlatitudes, J. Geophys. Res.-Atmos., 115, D05302, doi:10.1029/2009JD013351, 2010.
Laursen, K. K., Hobbs, P. V., Radke, L. F., and Rasmussen, R. A.: Some Trace Gas Emissions from North-American Biomass Fires with an Assessment of Regional and Global Fluxes from Biomass Burning, J. Geophys. Res., 97, 20687–20701, 1992.
Leung, F. Y. T., Logan, J. A., Park, R., Hyer, E., Kasischke, E., Streets, D., and Yurganov, L.:

ACPD
11, 5351–5378, 2011

Impacts of enhanced biomass burning in the boreal forests in 1998 on tropospheric chemistry and the sensitivity of model results to the injection height of emissions, J. Geophys. Res., 112, D10313, doi:10.1029/2006JD008132, 2007.

Mauzerall, D. L., Logan, J. A., Jacob, D. J., Anderson, B. E., Blake, D. R., Bradshaw, J. D., Heikes, B., Sachse, G. W., Singh, H., and Talbot, B.: Photochemistry in biomass burning plumes and implications for tropospheric ozone over the tropical South Atlantic, J. Geophys. Res., 103, 8401–8423, 1998.

McMeeking, G. R., Kreidenweis, S. M., Baker, S., Carrico, C. M., Chow, J. C., Collett, J. L., Hao, W. M., Holden, A. S., Kirchstetter, T. W., Malm, W. C., Moosmuller, H., Sullivan, A. P., and Wold, C. E.: Emissions of trace gases and aerosols during the open combustion of biomass in the laboratory, J. Geophys. Res., 114, D19210, doi:10.1029/2009JD011836, 2009.

Mesinger, F., DiMego, G., Kalnay, E., Mitchell, K., Shafran, P. C., Ebisuzaki, W., Jovic, D., Woollen, J., Rogers, E., Berbery, E. H., Ek, M. B., Fan, Y., Grumbine, R., Higgins, W., Li, H., Lin, Y., Manikin, G., Parrish, D., and Shi, W.: North American regional reanalysis, Bull. Am. Meteorol. Soc., 87, 343–360, 2006.

Pfister, G. G., Wiedinmyer, C., and Emmons, L. K.: Impacts of the fall 2007 California wildfires on surface ozone: Integrating local observations with global model simulations, Geophys. Res. Lett., 35, L19814, doi:10.1029/2008GL034747, 2008.

Real, E., Law, K. S., Weinzierl, B., Fiebig, M., Petzold, A., Wild, O., Methven, J., Arnold, S., Stohl, A., Huntrieser, H., Roiger, A., Schlager, H., Stewart, D., Avery, M., Sachse, G., Browell, E., Ferrare, R., and Blake, D.: Processes influencing ozone levels in Alaskan forest fire plumes during long-range transport over the North Atlantic, J. Geophys. Res., 112, D10S41, doi:10.1029/2006JD007576, 2007.

Seiler, W. and Crutzen, P. J.: Estimates of Gross and Net Fluxes of Carbon between the Biosphere and the Atmosphere from Biomass Burning, Clim. Change, 2, 207–247, 1980.

Spichtinger, N., Wenig, M., James, P., Wagner, T., Platt, U., and Stohl, A.: Satellite detection of a continental-scale plume of nitrogen oxides from boreal forest fires, Geophys. Res. Lett., 28, 4579-4582, 2001.

Val Martin, M., Honrath, R. E., Owen, R. C., Pfister, G., Fialho, P., and Barata, F.: Significant enhancements of nitrogen oxides, black carbon, and ozone in the North Atlantic lower free troposphere resulting from North American boreal wildfires, J. Geophys. Res., 111, D23S60, doi:10.1029/2006JD007530, 2006.

van Leeuwen, T. T. and van der Werf, G. R.: Spatial and temporal variability in the ratio of

ACPD
11, 5351–5378, 2011

trace gases emitted from biomass burning, Atmos. Chem. Phys. Discuss., 10, 23559–23599, doi:10.5194/acpd-10-23559-2010, 2010.
Vermote, E., Ellicott, E., Dubovik, O., Lapyonok, T., Chin, M., Giglio, L., and Roberts, G. J.: An approach to estimate global biomass burning emissions of organic and black carbon from MODIS fire radiative power, J. Geophys. Res., 114, D18205, doi:10.1029/2008JD011188, 2009.
Wiedinmyer, C., Quayle, B., Geron, C., Belote, A., McKenzie, D., Zhang, X. Y., O'Neill, S., and Wynne, K. K.: Estimating emissions from fires in North America for air quality modeling, Atmos. Environ., 40, 3419–3432, 2006.
Wooster, M. J.: Small-scale experimental testing of fire radiative energy for quantifying mass combusted in natural vegetation fires, Geophys. Res. Lett., 29, 2027, doi:10.1029/2002GL015487, 2002.
Wooster, M. J., Zhukov, B., and Oertel, D.: Fire radiative energy for quantitative study of biomass burning: derivation from the BIRD experimental satellite and comparison to MODIS fire products, Remote Sens. Environ., 86, 83–107, 2003.
Wooster, M. J., Roberts, G., Perry, G. L. W., and Kaufman, Y. J.: Retrieval of biomass combustion rates and totals from fire radiative power observations: FRP derivation and calibration relationships between biomass consumption and fire radiative energy release, J. Geophys. Res., 110, D24311, doi:10.1029/2005JD006318, 2005.
Yokelson, R. J., Goode, J. G., Ward, D. E., Susott, R. A., Babbitt, R. E., Wade, D. D., Bertschi, I., Griffith, D. W. T., and Hao, W. M.: Emissions of formaldehyde, acetic acid, methanol, and other trace gases from biomass fires in North Carolina measured by airborne Fourier transform infrared spectroscopy, J. Geophys. Res.-Atmos., 104, 30109–30125, 1999.
Yokelson, R. J., Urbanski, S. P., Atlas, E. L., Toohey, D. W., Alvarado, E. C., Crounse, J. D., Wennberg, P. O., Fisher, M. E., Wold, C. E., Campos, T. L., Adachi, K., Buseck, P. R., and Hao, W. M.: Emissions from forest fires near Mexico City, Atmos. Chem. Phys., 7, 5569–5584, doi:10.5194/acp-7-5569-2007, 2007.
Yokelson, R. J., Christian, T. J., Karl, T. G., and Guenther, A.: The tropical forest and fire emissions experiment: laboratory fire measurements and synthesis of campaign data, Atmos. Chem. Phys., 8, 3509–3527, doi:10.5194/acp-8-3509-2008, 2008.
Zhang, X. Y. and Kondragunta, S.: Temporal and spatial variability in biomass burned areas across the USA derived from the GOES fire product, Remote Sens. Environ., 112, 2886–2897, 2008.

ACPD
11, 5351–5378, 2011

Table 1. NO_2 and NO_x ECs and NO_x EFs by fuel type.

Land type	NO_2 EC ($g\,MJ^{-1}$)	NO_x EF ($g\,kg^{-1}$)[a,b]	NO_x EC ($g\,MJ^{-1}$)[a]
Forest	0.279 ± 0.077	0.59 ± 0.16	0.243 ± 0.067
Grass	0.342 ± 0.053	0.73 ± 0.11	0.297 ± 0.046
Shrub	0.696 ± 0.088	1.48 ± 0.19	0.605 ± 0.077

Reported uncertainties are 1σ, calculated via nonparametric bootstrap resampling.
[a] assumes NO_2/NO_x of 0.75. Total NO_x mass expressed as NO.
[b] assumes $K_R = 0.41\,kg\,MJ^{-1}$

ACPD
11, 5351–5378, 2011

Table 2. Possible biases in this analysis.

Possible biases	Bias range (%)	Bias direction
Assumed NO_x lifetime	0–20	Indeterminate
NO_2/NO_x ratio	0–20	Indeterminate
Value for K	0–15	Indeterminate
FRP overestimation due to diurnal fire cycle	15–20	Negative
FRP underestimation due to clouds/smoke/canopy	15–30	Positive
Increased flaming sampling due to diurnal fire cycle	10–20	Positive
Emissions from CA/NV are lower than global average	Indeterminate	Indeterminate
Bias in OMI retrieval	Indeterminate	Indeterminate

ACPD
11, 5351–5378, 2011

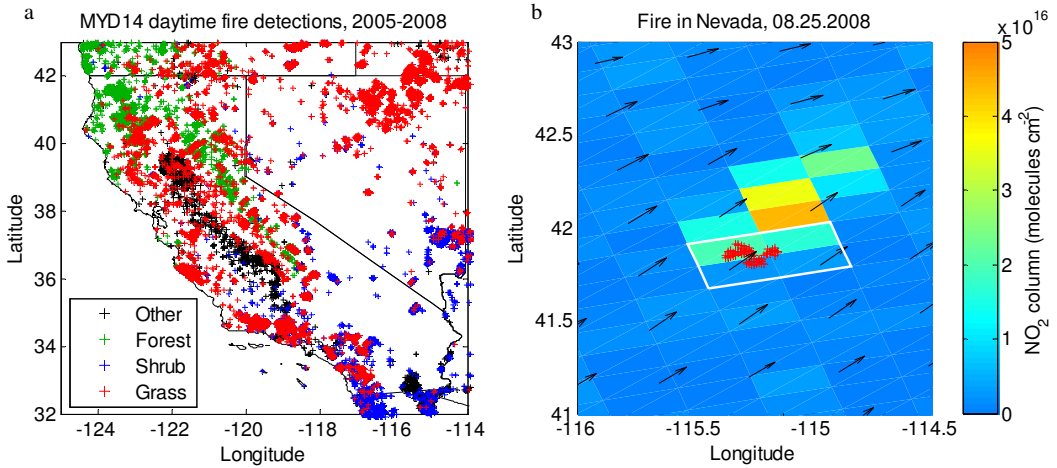

Fig. 1. (a) MODIS fire detections (totaling $\sim 2.8 \times 10^4$ 1 km pixels) from the daytime EOS-Aqua overpass over California and Nevada, for 2005–2008, colored by land type. **(b)** Fire detected in Nevada on 25 August 2008, illustrating NO_2 fire plume as seen by OMI. Shown are OMI tropospheric NO_2 column densities (molecules cm^{-2}), overlayed with MODIS fire detections (red) and NARR wind vectors (black arrows); OMI pixels analyzed for this fire are outlined in white. Average wind speed shown is 8.23 m s^{-1}.

ACPD
11, 5351–5378, 2011

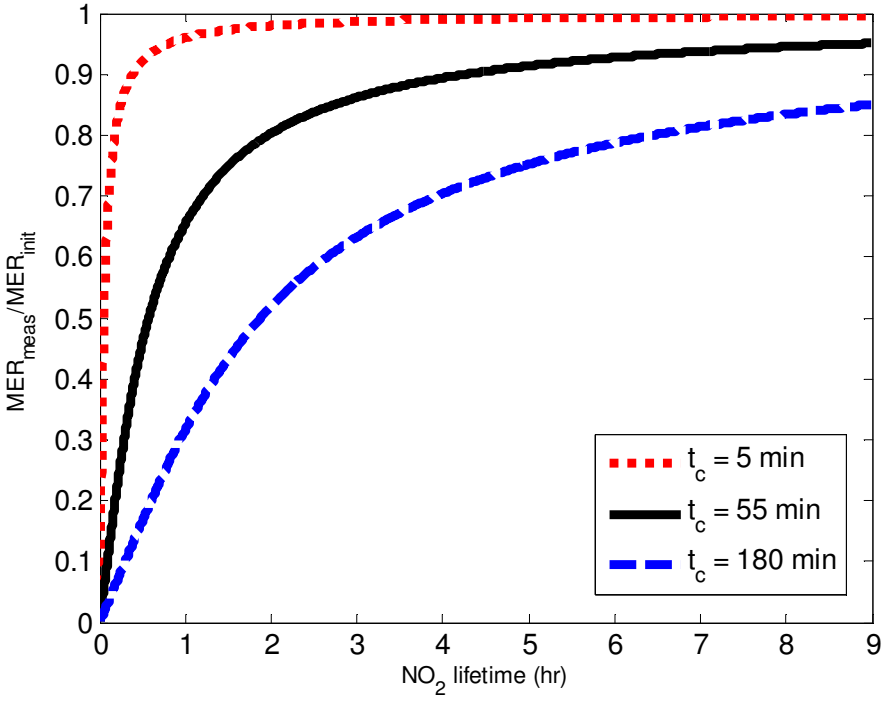

Fig. 2. The NO_2 mass emission rate (MER) measured in this analysis (as a fraction of the initial MER from the fire) vs. NO_x lifetime in the plume (Eq. 10) for three sample clear times in our analysis: the shortest (5 min), average (55 min) and longest (180 min).

ACPD
11, 5351–5378, 2011

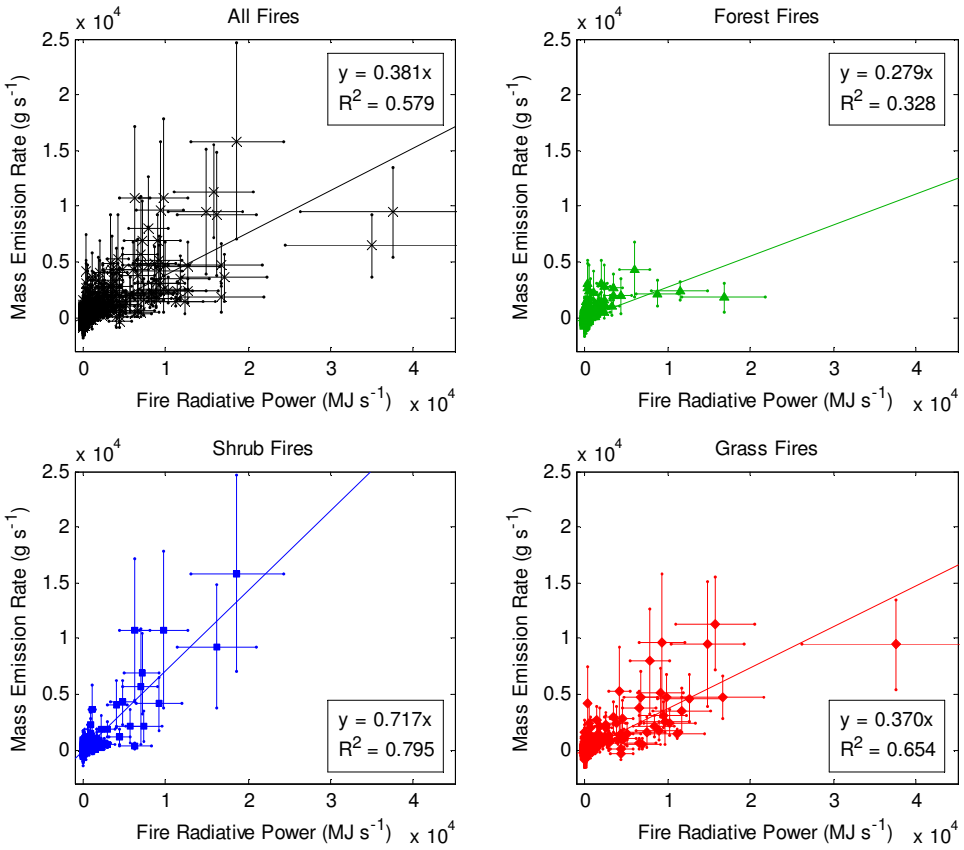

Fig. 3. Plots of fire radiative power (FRP) vs. NO_2 mass emission rate (MER) for fires grouped by land type: all **(a)**, forests **(b)**, shrubs **(c)**, and grasses **(d)**, with lines of best fit and R^2 values. Error bars are one standard deviation for MER and range for FRP as reported in the text.

ACPD
11, 5351–5378, 2011

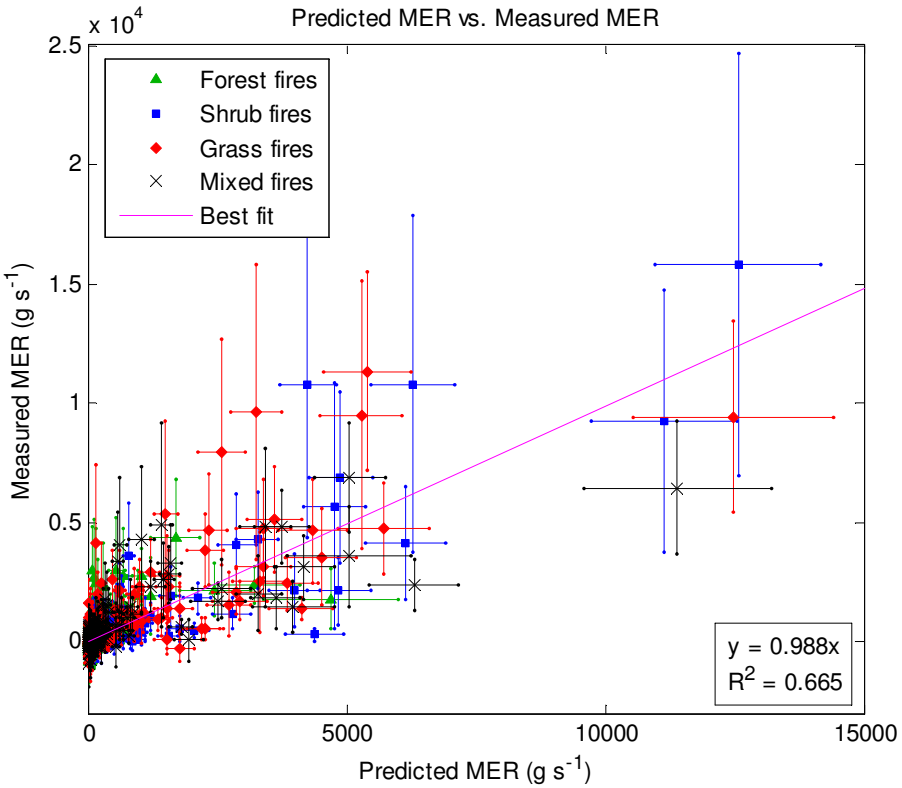

Fig. 4. Predicted NO_2 mass emission rate (MER), calculated using fire radiative power and the multiple regression coefficients, vs. MER measured in the analysis. Error bars in measured MER are one standard deviation, calculated as reported; error bars in predicted MER are calculated using one standard deviation of each calculated emission coefficient.

ACPD
11, 5351–5378, 2011